

# Experiments and Modeling of Autoignition of Methyl Valerate at Low to Intermediate Temperatures and Elevated Pressures in a Rapid Compression Machine

Bryan W. Weber<sup>a,\*</sup>, Justin A. Bunnell<sup>a</sup>, Kamal Kumar<sup>b</sup>, Chih-Jen Sung<sup>a</sup>

<sup>a</sup>*Department of Mechanical Engineering, University of Connecticut, Storrs, CT, USA*

<sup>b</sup>*Department of Mechanical Engineering, University of Idaho, Moscow, ID, USA*

---

## Abstract

Methyl valerate ( $\text{C}_6\text{H}_{12}\text{O}_2$ , methyl pentanoate) is a methyl ester and a relevant surrogate component for biodiesel. In this work, we present ignition delays of methyl valerate measured using a rapid compression machine at a range of engine-relevant temperature, pressure, and equivalence ratio conditions. The conditions we have studied include equivalence ratios ( $\phi$ ) from 0.25 to 2.0, temperatures between 680 K and 1050 K, and pressures of 15 bar and 30 bar. The ignition delay data demonstrate a negative temperature coefficient region in the temperature range of 720 K–800 K for both  $\phi = 2.0$ , 15 bar and  $\phi = 1.0$ , 30 bar, with two-stage ignition apparent over the narrower temperature ranges of 720 K–760 K for 15 bar and 740 K–760 K at 30 bar. In addition, the experimental ignition delay data are compared with simulations using an existing chemical kinetic model from the literature. The simulations with the literature model under-predict the data by factors between 2 and 10 over the entire range of the experimental data. In addition, a new chemical kinetic model is developed using the Reaction Mechanism Generator (RMG) software. The agreement between the experimental data and the RMG model is also not satisfactory. To help determine the possible reasons for the disagreement, a path analysis of both models is completed. It is found that improvements to both the reaction pathways and thermodynamic properties are required. Further directions for

---

\*Corresponding Author: bryan.weber@uconn.edu

future improvement of the methyl valerate model are discussed.

*Keywords:* chemical kinetics, rapid compression machine, autoignition, methyl ester, methyl valerate, methyl pentanoate

---

## 1. Introduction

For transportation applications, biodiesel is an important constituent in improving environmental friendliness of fuels. This is due to its renewability when produced from sustainable agricultural crops and its ability to reduce emissions relative to petroleum-derived fuels [1]. Biodiesel typically consists of long-chain methyl ester molecules, with typical compositions of  $C_{14}$  to  $C_{20}$  [1]. Recognizing that the large molecular size of the methyl esters within biodiesel fuel makes creating and using detailed chemical kinetic models challenging [2], it is desired to study their combustion chemistry by studying simpler methyl ester molecules.

A recent review paper summarizes the work on methyl esters relevant to biodiesel combustion [3]; the following summary focuses on ignition delay measurements, since these are the focus of this paper. Autoignition of methyl butanoate (MB,  $C_5H_{10}O_2$ ) has been well-studied in both shock tube and rapid compression machine experiments [4–10]. The prevalence of MB data in the literature is largely due to the early identification of MB as a potential surrogate fuel for biodiesel [11]. However, the experiments have shown that MB may not be an appropriate surrogate for biodiesel, due to its lack of negative temperature coefficient (NTC) behavior, a requirement for a suitable biodiesel surrogate [3].

Methyl esters larger than MB, such as methyl valerate (MV,  $C_6H_{12}O_2$ , methyl pentanoate), have also been studied as possible biodiesel surrogates. Hadj-Ali et al. [9] used a rapid compression machine (RCM) to study the autoignition of several methyl esters including MV. Although MV exhibited two-stage ignition in this study, little additional research has been done on its low-temperature chemistry. Korobeinichev et al. [12] studied MV in premixed laminar flames and extended a detailed high temperature chemical kinetic model

27 to include MV and methyl hexanoate. Dmitriev et al. [13] added MV to n-  
 28 heptane/toluene fuel blends to determine the resulting intermediate species in  
 29 premixed flames using a flat burner at 1 atm and an equivalence ratio of 1.75.  
 30 The addition of MV helped reduce soot forming intermediates including ben-  
 31 zene, cyclopentadienyl, acetylene, propargyl, and vinylacetylene [13]. Hayes  
 32 and Burgess [14] computationally examined the peroxy radical isomerization  
 33 reactions for MV to better understand the low temperature reaction pathways.  
 34 Finally, Diévert et al. [15] used diffusion flames in the counterflow configuration  
 35 to determine extinction limits for a number of methyl esters, including MV, and  
 36 validated a detailed kinetic model with the experimental data.

37 This work provides additional data for the autoignition of MV. Data is col-  
 38 lected in a RCM under engine relevant conditions spanning from 15 bar to 30 bar,  
 39 equivalence ratios ( $\phi$ ) from 0.25 to 2.0, and temperatures from 680 K to 1050 K.  
 40 The NTC region of MV is mapped out to provide additional information on the  
 41 fidelity of using MV as a biodiesel surrogate.

## 42 **2. Experimental Methods**

43 The RCM used in this study is a single piston arrangement and is pneu-  
 44 matically driven and hydraulically stopped. The device has been described in  
 45 detail previously [16] and will be described here briefly for reference. The end  
 46 of compression (EOC) temperature and pressure ( $T_C$  and  $P_C$  respectively), are  
 47 independently changed by varying the overall compression ratio, initial pressure  
 48 ( $P_0$ ), initial temperature ( $T_0$ ), and specific heat ratio of the experiments. The  
 49 piston in the reaction chamber is machined with a specially designed crevice to  
 50 suppress the roll-up vortex effect and promote homogeneous conditions in the  
 51 reactor during and after compression [17].

52 The primary diagnostic on the RCM is the in-cylinder pressure measured by  
 53 a Kistler 6125C dynamic transducer that is compensated for thermal shock. The  
 54 transducer is coupled to a Kistler 5010B charge amplifier. The voltage output  
 55 of the charge amplifier is recorded by a National Instruments 9125 analog input

device connected to a cDAQ 9178 chassis. The voltage is sampled at a rate of either 50 kHz or 100 kHz by a LabView VI and processed by a Python package called UConnRCMPy [18]. Version 3.0.5 of UConnRCMPy [19], 3.6 of Python, 2.3.0 of Cantera [20], 1.13 of NumPy [21], 0.19.0 of SciPy [22], and 2.0.1 of Matplotlib [23] are used in the analysis in this paper.

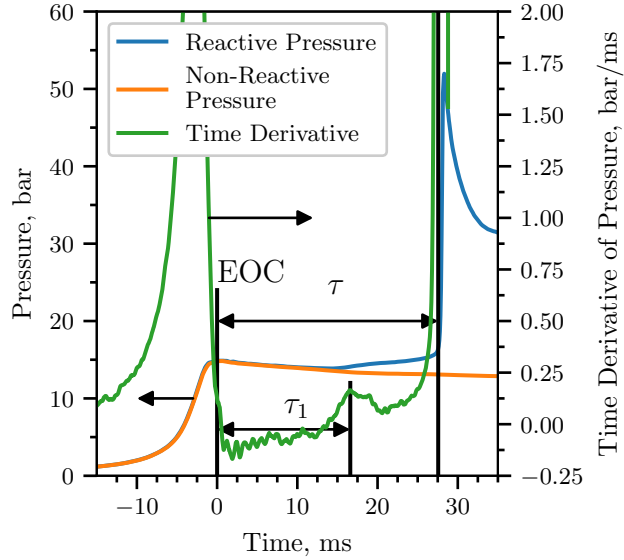


Figure 1: Definition of the ignition delays used in this work. The experiment in this figure is conducted for a  $\phi = 2.0$  mixture with  $\text{Ar}/(\text{N}_2 + \text{Ar}) = 0.5$ ,  $P_0 = 0.7806$  bar,  $T_0 = 373$  K,  $P_C = 14.92$  bar,  $T_C = 720$  K,  $\tau = (27.56 \pm 0.89)$  ms, and  $\tau_1 = (16.60 \pm 0.46)$  ms.

The compression stroke of the RCM brings the fuel/oxidizer mixture to the EOC conditions, and for suitable thermodynamic states, the mixture will ignite after a delay period. The definitions of the ignition delays are shown in Fig. 1. The time of the EOC is defined as the maximum of the pressure trace prior to the start of ignition and the ignition delays are defined as the time from the EOC until local maxima in the first time derivative of the pressure. Each experimental condition is repeated at least five times to ensure repeatability of the data. As there is some random scatter present in the data, the standard deviation ( $\sigma$ ) of the ignition delays from the runs at a given condition is computed. Typically,

$\sigma$  is less than 10 % of the mean values of the overall ignition delay ( $\tau$ ) and the first stage ignition delay ( $\tau_1$ ).

In addition to the reactive experiments, non-reactive experiments are conducted by replacing  $O_2$  with  $N_2$  to determine the influence of machine-specific behavior on the experimental conditions and permit the calculation of the EOC temperature via the isentropic relations between pressure and temperature [24]. The EOC temperature is calculated by the procedure described in Section 3.

The mixtures considered in this study are shown in Table 1. Four equivalence ratios of MV in “air” are considered. While  $O_2$  is kept at 21 % by mole in the oxidizer, the ratio of Ar :  $N_2$  in the oxidizer is varied to adjust the temperatures reached at the EOC. Two  $P_C$  conditions are studied in this work, 15 bar and 30 bar, representing engine-relevant conditions. For the  $\phi = 2.0$  condition, only  $P_C = 15$  bar is considered because we could not achieve  $T_C$  values low enough that the ignition during the compression stroke can be prevented.

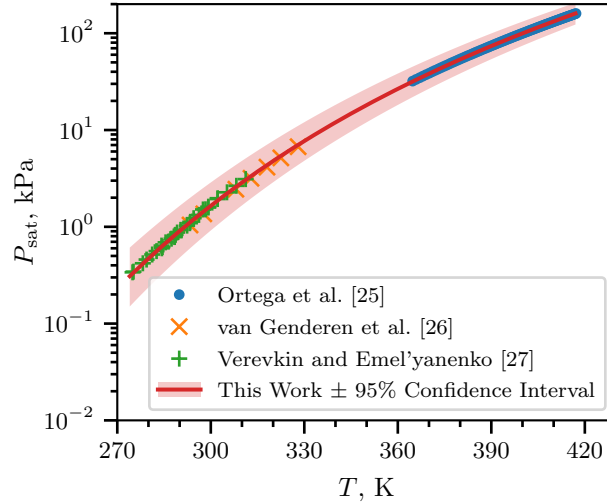
Table 1: Mixtures considered in this work

| $\phi$ | Mole Fraction (purity) |                  |               |                  | Ar/( $N_2 + Ar$ ) |
|--------|------------------------|------------------|---------------|------------------|-------------------|
|        | MV (100 %)             | $O_2$ (99.994 %) | Ar (99.999 %) | $N_2$ (99.999 %) |                   |
| 0.25   | 0.0065                 | 0.2087           | 0.7848        | 0.0000           | 1.0               |
| 0.5    | 0.0130                 | 0.2074           | 0.7796        | 0.0000           | 1.0               |
| 1.0    | 0.0256                 | 0.2047           | 0.7697        | 0.0000           | 1.0               |
| 1.0    | 0.0256                 | 0.2047           | 0.3849        | 0.3848           | 0.5               |
| 2.0    | 0.0499                 | 0.1996           | 0.0000        | 0.7505           | 0.0               |
| 2.0    | 0.0499                 | 0.1996           | 0.3752        | 0.3753           | 0.5               |

Mixtures are prepared in stainless steel mixing tanks, 17 L and 15 L in size. The proportions of reactants in the mixture are determined by specifying the absolute mass of the fuel, the equivalence ratio, and the ratio of Ar :  $N_2$  in the oxidizer. Mixtures are made by first vacuuming the mixing tanks to an ultimate pressure less than 5 Torr. Since MV is a liquid with a relatively small

95 vapor pressure at room temperature and pressure, it is measured gravimetrically  
 96 to within 0.01 g of the specified value. The fuel is injected into the mixing tank  
 97 through a septum. Proportions of O<sub>2</sub>, Ar, and N<sub>2</sub> are added manometrically at  
 98 room temperature and the total pressure is measured by an Omega Engineering  
 99 MMA100V10T2D0T4A6 type static pressure transducer. The same transducer  
 100 is used to measure the pressure of the reactants prior to an experiment.

101 The RCM is equipped with heaters to control the initial temperature of the  
 102 mixture. After filling in the components to the mixing tanks, the heaters are  
 103 switched on and the system is allowed 1.5 h to come to steady state. The mixing  
 104 tanks are also equipped with magnetic stir bars so the reactants are well mixed  
 105 for the duration of the experiments.



106

Figure 2: Saturated vapor pressure of MV as a function of temperature, plotted using the  
 107 Antoine equation, Eq. (1), with  $A = 6.4030$ ,  $B = 1528.69$ , and  $C = 52.881$ .

The initial temperature is chosen such that the saturated vapor pressure ( $P_{\text{sat}}$ ) of the fuel at the initial temperature is at least twice the partial pressure of the fuel in the mixing tank. The Antoine equation

$$\log_{10} P_{\text{sat}} = A - \frac{B}{T - C} \quad (1)$$

is used to model the saturated vapor pressure of MV as a function of temperature ( $T$ ), where  $A$ ,  $B$ , and  $C$  are substance-specific coefficients. Coefficients for Eq. (1) are given in the literature by Ortega et al. [25], Camacho et al. [28], and Stephenson et al. [29]. Unfortunately, the values of the coefficients are different among all three references. Therefore, coefficients for use in Eq. (1) are determined in this work by least squares fitting of the data of Ortega et al. [25], van Genderen et al. [26], and Verevkin and Emel’yanenko [27] using the `curve_fit()` function of SciPy [22] version 0.19.0. Figure 2 shows that the coefficients fitted with this procedure give good agreement with the experimental data; values for the coefficients computed in this work and in the literature works are given in Table 2. The data used to calculate the coefficients are provided in the Supplementary Material.

Table 2: Antoine Equation coefficients computed in this work and from the literature. The  $2\sigma$  confidence interval is estimated by taking the square root of the diagonals of the covariance matrix returned from `curve_fit()`

|                               | $A$     | $B$     | $C$    | $T_{\min}$ , K | $T_{\max}$ , K |
|-------------------------------|---------|---------|--------|----------------|----------------|
| This Work                     | 6.4030  | 1528.69 | 52.881 | 274.9          | 417.18         |
| $2\sigma$ Confidence Interval | 0.0919  | 53.47   | 4.934  | —              | —              |
| Ortega et al. [25]            | 6.23175 | 1429.00 | 62.30  | 364.75         | 417.18         |
| Camacho et al. [28]           | 5.9644  | 1281.06 | 75.94  | 281            | 547            |
| Stephenson et al. [29]        | 6.62646 | 1658.4  | 42.09  | 297            | 411            |

### 3. Computational Methods

#### 3.1. RCM Modeling

The Python 3.6 interface of Cantera [20] version 2.3.0 is used for all simulations in this work. Detailed descriptions of the use of Cantera for these simulations can be found in the work of Weber and Sung [18] and Dames et al. [30]; a brief overview is given here. As mentioned in Section 2, non-reactive experiments are conducted to characterize the machine-specific effects on the

129 experimental conditions in the RCM. This pressure trace is combined with the  
 130 reactive pressure trace and used to compute a volume trace by assuming that  
 131 the reactants undergo a reversible, adiabatic, constant composition (i.e., isen-  
 132 tropic) compression during the compression stroke and an isentropic expansion  
 133 after the EOC. The volume trace is applied to a simulation conducted in an  
 134 `IdealGasReactor` in Cantera [20] using the CVODES solver from the SUN-  
 135 DIALS suite [31]. The ignition delays from the simulations are defined in the  
 136 same manner as in the experiments. The time derivative of the pressure in the  
 137 simulation is computed by second order Lagrange polynomials, as discussed by  
 138 Chapra and Canale [32].

139 To the best of our knowledge, there are three mechanisms for MV com-  
 140 bustion available in the literature. The first two, by Korobeinichev et al. [12]  
 141 and Dmitriev et al. [13], were developed to simulate flames, and do not include  
 142 the low-temperature chemistry necessary to simulate the conditions in these ex-  
 143 periments. The third model was developed by Diévar et al. [15] and includes  
 144 low-temperature chemistry of MV, although it was only validated by comparison  
 145 with flame extinction limits. In converting this mechanism for use in Cantera,  
 146 we found that there were many species in the thermodynamic database with  
 147 multiple data entries. For most of these species the thermodynamic data is  
 148 identical. However, some species are not exact duplicates. For these species, it  
 149 is not clear from the thermodynamic database file which data set should be pre-  
 150 ferred. Since Cantera (and CHEMKIN) choose the first instance of a duplicate  
 151 species to be used, we retained the first entry for all duplicated species. The  
 152 detailed model of Diévar et al. [15] includes 1105 species and 7141 reactions,  
 153 and the Cantera formatted input file is available in the Supplementary Material.

### 154 *3.2. Reaction Mechanism Generator*

155 In addition to using a mechanism from the literature, we investigate the use  
 156 of an automatic mechanism generator, the open-source Reaction Mechanism  
 157 Generator (RMG) [33] version 2.1.0. The Python version of RMG is used,  
 158 which requires Python 2.7, and version 2.1.0 of the RMG database is used.



159 The final RMG model contains 427 species and 13640 reactions. Note that the  
 160 number of species is much lower than the Diévar et al. [15] model because  
 161 the RMG model focuses on only one fuel (MV), but the number of reactions is  
 162 substantially higher. The input file used to generate the model is available in the  
 163 Supplementary Material. In addition, the CHEMKIN and Cantera formatted  
 164 input files for the RMG model are available in the Supplementary Material.

## 165 4. Experimental Results

### 166 4.1. Ignition Delays

167 Figure 3 shows the ignition delay results measured in this study. Filled  
 168 markers denote the overall ignition delay and hollow markers indicate the first-  
 169 stage ignition delay. Vertical error bars are drawn on the symbols to represent  
 170 the  $2\sigma$  uncertainty in the ignition delay; for many of the experiments, the un-  
 171 certainty is approximately the same size as the data point, so the error bar is  
 172 hidden. Horizontal error bars are shown on the first and last points of each  
 173 equivalence ratio indicating the estimated uncertainty in the EOC temperature  
 174 of  $\pm 1\%$  [34]. Fig. 3a shows the results for a compressed pressure of 15 bar,  
 175 while Fig. 3b shows the results for a compressed pressure of 30 bar. Note that  
 176  $\phi = 2.0$  results were not collected for 30 bar, so there are no red triangle data  
 177 points in Fig. 3b. All the data are available in comma-separated value files and  
 178 ChemKED-format [35] files in the Supplementary Material.

179 It can be seen from Fig. 3 that the ignition delays for the  $\phi = 0.25$  and 0.5  
 180 mixtures do not show an NTC region of the ignition delay for both of the  
 181 pressures studied in this work. However, the  $\phi = 1.0$  mixture shows an NTC  
 182 region at  $P_C = 30$  bar between approximately 720 K and 800 K, with measured  
 183 first-stage ignition delays at 733 K and 757 K. In addition, the  $\phi = 2.0$  mixture  
 184 shows an NTC region of ignition delay at 15 bar from approximately 720 K to  
 185 780 K, with measured first-stage ignition delays between 720 K and 750 K.

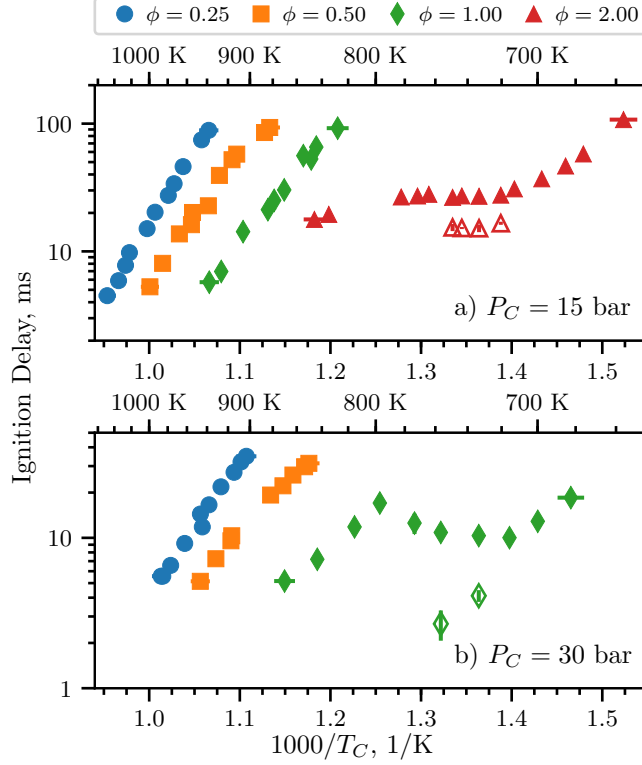


Figure 3: Ignition delays of MV as a function of inverse temperature for varying equivalence ratios. Filled points are the overall ignition delays and hollow points are the first stage ignition delays. a) 15 bar, b) 30 bar.

Hadj-Ali et al. [9] also observed two-stage ignition of MV in stoichiometric mixtures, stating that “[m]ethyl pentanoate... was more reactive [than methyl butanoate] with a limit below which autoignition no longer occurs observed at  $T_c = 670$  K and  $P_c = 11.4$  bar. At this temperature, the autoignition occurred in two stages with a clearly identified cool flame event.” However, we do not find two stage ignition for the similar pressure of  $P_C = 15$  bar in this study. We note that the stated temperature of the experiment from the work of Hadj-Ali et al. [9] (670 K) is much lower than the lowest temperature we considered in this work at 15 bar,  $\phi = 1.0$  (828 K). We did not conduct experiments at lower temperatures because the work of Mittal and Sung [17] showed that the

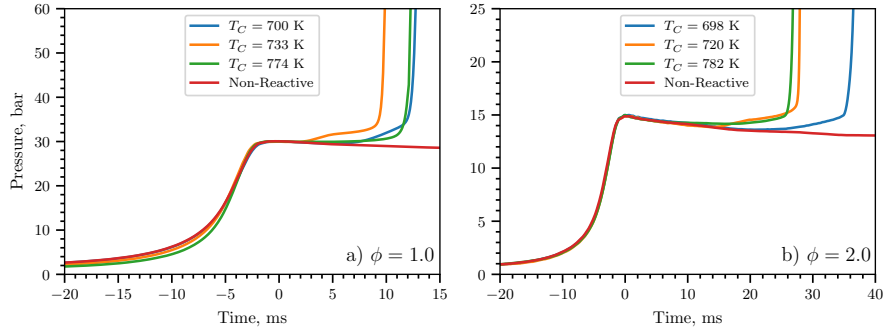
198 temperature field in the RCM reaction chamber was uniform for approximately  
199 100 ms after the EOC, and our measured ignition delay at 15 bar,  $\phi = 1.0$ , and  
200 828 K is 92.14 ms.

201 However, we note NTC behavior of the ignition delay and two-stage igni-  
202 tion at the higher pressure of 30 bar, and at higher temperatures than those  
203 reported for two-stage ignition in the study of Hadj-Ali et al. [9]. The trend  
204 of NTC behavior shifting to higher temperatures with increasing pressure can  
205 be seen in other classes of fuels. Kukkadapu et al. [36] found a similar trend  
206 in gasoline composed of iso-alkanes, n-alkanes, cyclo-alkanes, aromatics, and  
207 olefins. Kukkadapu et al. [36] attributed the shift of the NTC region to the re-  
208 actions between the hydroperoxyalkyl radical (QOOH) and  $O_2$  becoming more  
209 dominant than the unimolecular decomposition of QOOH at higher pressures.  
210 Similar trends could occur for the hydroperoxyalkyl radicals of MV.

211 To further understand the effect of the methyl ester functional group on the  
212 NTC region of ignition delay, we compare with the alkane and alcohol with  
213 5-carbon alkyl chains, n-pentane and n-pentanol. n-Pentane and MV have the  
214 same fuel mole percentage for stoichiometric mixtures in air (2.56 %), while  
215 n-pentanol has a fuel mole percentage of 2.72 % for stoichiometric conditions.  
216 Ribaucour et al. [37] and Bugler et al. [38] found the NTC region for n-pentane  
217 to be between 760 K and 910 K at pressures near 10 atm. As we will compare  
218 with our MV data at 30 bar, we note that increasing the pressure tends to shift  
219 the NTC to higher temperatures, as mentioned previously [36]. Heufer et al. [39]  
220 found NTC behavior for n-pentanol in the range of 770 K to 900 K at 30 bar. In  
221 this study, we find the NTC window for MV at 30 bar to be between 720 K and  
222 800 K. Therefore, it appears that the methyl ester functional group causes the  
223 NTC range to occur at lower temperature as compared to alkanes and alcohols  
224 with similar alkyl chain lengths. This result was also noted by Hadj-Ali et al.  
225 [9] for methyl hexanoate as the fuel.

#### 226 4.2. Pressure Traces

227 Figure 4a shows the pressure traces for selected experiments at  $\phi = 1.0$ ,  $P_C =$   
 228 30 bar. The three reactive pressure traces shown are at the low-temperature end  
 229 of the NTC (blue, 700 K), one case with two-stage ignition (orange, 733 K), and  
 230 one case near the high-temperature limit of the NTC region (green, 774 K). Also  
 231 shown is the non-reactive pressure trace for the 700 K case (red). By comparing  
 232 the 700 K pressure trace with the non-reactive pressure trace, it can be seen  
 233 that there is substantial heat release prior to main ignition as measured by the  
 234 deviation of the reactive pressure trace from the non-reactive trace. However,  
 235 there is only one peak in the time derivative of the pressure, so no first-stage  
 236 ignition delay is defined for this case. It can also be seen in Fig. 4a that the  
 237 774 K case shows some heat release prior to ignition, although again there is  
 238 only one peak in the time derivative of the pressure. Furthermore, the heat  
 239 release at 774 K appears to be more gradual than at 700 K.



240 Figure 4: Selected pressure traces around the NTC region of ignition delay. a)  $\phi = 1.0$ ,  $P_C =$   
 241 30 bar b)  $\phi = 2.0$ ,  $P_C = 15$  bar

242 A similar trend can be observed in Fig. 4b for  $\phi = 2.0$  at  $P_C = 15$  bar,  
 243 where pressure traces at several points around the NTC region are plotted. As  
 244 in Fig. 4a, the three reactive pressure traces shown are at the low-temperature  
 245 end of the NTC (blue, 698 K), one case with two-stage ignition (orange, 720 K),  
 246 and one case near the high-temperature limit of the NTC region (green, 782 K).  
 247 Also shown is the non-reactive pressure trace for the 698 K case (red). As for

the  $\phi = 1.0$  case, the pressure traces show significant heat release prior to the overall ignition, as judged by deviation from the non-reactive case.

## 5. Computational Results

Figure 5 compares experimentally measured overall ignition delays with ignition delays computed with the detailed model of Diévert et al. [15] (solid lines). Figure 5a shows results at  $P_C = 15$  bar, while Fig. 5b shows results at  $P_C = 30$  bar. Only some equivalence ratios are shown for each pressure condition; data and simulated results are not shown for cases where the reactive simulated temperature at the EOC deviated substantially from the non-reactive temperature due to heat release during the compression stroke. Furthermore, it is important to note that the model of Diévert et al. [15] was not validated for MV ignition delays, only for extinction strain rates.

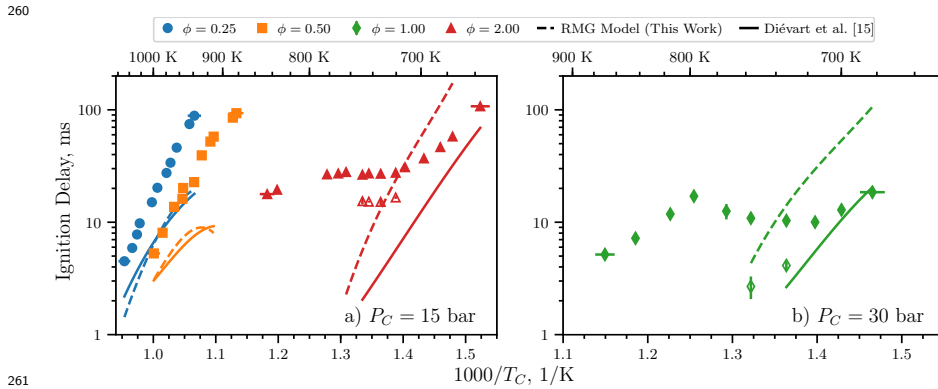


Figure 5: Comparison of experimental and simulated results. a) 15 bar; b) 30 bar

At 15 bar, the experimental ignition delays are under-predicted by the Diévert et al. [15] model for the three equivalence ratios shown. For the  $\phi = 0.25$  and 0.5 conditions, the model appears to be predicting an NTC region of the ignition delays as the temperature decreases, although such a trend is not observed in the data. However, at  $\phi = 2.0$ , the model does not predict the presence of an NTC region, although one is present in the experiments. Nonetheless, the agreement

269 seems to be improving as the temperature is decreased. Comparing the Diévert  
 270 et al. [15] model to the stoichiometric data at 30 bar, we find a similar trend as  
 271 the  $\phi = 2.0$ ,  $P_C = 15$  bar data. The model does not predict the NTC region  
 272 found experimentally for the  $\phi = 1.0$  experiments, but the agreement improves  
 273 as the temperature decreases. Interestingly, two-stage ignition is predicted for  
 274 all of the  $\phi = 1.0$  and  $\phi = 2.0$  data shown in Fig. 5. However, the first-stage  
 275 ignition delays are 0.1 ms to 0.5 ms less than the overall ignition delays, and are  
 276 not shown on Fig. 5 because they are nearly indistinguishable from the overall  
 277 ignition delay. While the model of Diévert et al. [15] over-predicts the first-stage  
 278 ignition delay, it also over-predicts the first-stage pressure rise, thereby leading  
 279 to rapid overall ignition.

280 To elucidate the underlying reasons for the disagreement between the Diévert  
 281 et al. [15] model and the data, we constructed an additional model using RMG  
 282 (see Section 3.2). As can be seen in Fig. 5a, the agreement between the RMG  
 283 model (dashed lines) and the experimental data is similar to the Diévert et al.  
 284 [15] model for the 15 bar,  $\phi = 0.25$  and 0.5 data. Moreover, the RMG model  
 285 predicts a similar NTC region as temperature is decreasing. For the 15 bar,  
 286  $\phi = 2.0$  data, the RMG model tends to over-predict the low-temperature ignition  
 287 delays, and does not predict the NTC region found experimentally. As before,  
 288 the trend at 30 bar,  $\phi = 1.0$  is similar to the 15 bar,  $\phi = 2.0$  data; the RMG  
 289 model over-predicts the low-temperature ignition delays and does not predict  
 290 the experimental NTC region. Finally, as in the Diévert et al. [15] model, two-  
 291 stage ignition is predicted for all of the  $\phi = 1.0$  and  $\phi = 2.0$  data shown in  
 292 Fig. 5. However, the first-stage ignition delays are 0.1 ms to 0.5 ms less than  
 293 the overall ignition delays, and are not shown on Fig. 5 because they are nearly  
 294 indistinguishable from the overall ignition delay. Again, the over-prediction of  
 295 the first-stage ignition delay and pressure rise requires further investigation and  
 296 understanding of the complex low-temperature chemistry.

297 It is clear that neither model is able to predict the ignition delays of MV  
 298 particularly well. In addition to the poor agreement shown in Fig. 5, the simu-  
 299 lations for  $P_C = 15$  bar,  $\phi = 1.0$  and  $P_C = 30$  bar,  $\phi = 0.25$ , 0.5 and 2.0 showed

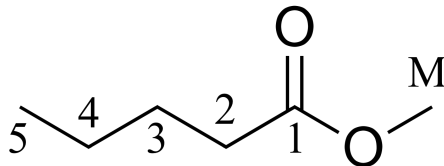
substantial heat release during the compression stroke (i.e., the simulations are much too reactive), and so these conditions aren't compared in Fig. 5. We note again that the model by Diévar et al. [15] was validated for MV combustion only by comparison to flame extinction limits, so the disagreement is not wholly surprising.

In general, there could be three likely sources of error in the models: missing reaction pathways, incorrect values of the reaction rates, and incorrect values for thermodynamic properties of the species. We have noted in Section 3.2 that the RMG model has many more reactions than the Diévar et al. [15] model and the algorithm used in RMG considers a substantial number of the possible pathways. This reduces the possibility of missing reaction pathways affecting the model. Further detailed studies are required to ensure that the RMG model includes all of the relevant reaction pathways, which are outside the scope of this work.

The second source of error may be incorrect reaction rate parameters, either because the rates are specified incorrectly in the model or because the rates are not well estimated by the typical analogy based-rules. It should be noted that errors of this type may affect the model generated by RMG—if the rates are not estimated correctly, reactions that are important in reality may not be included in the model. Determining the accuracy of the reaction rates used in the RMG and Diévar et al. [15] models requires further detailed studies of the models, which are also outside the scope of this work. Another, related, source of error could be incorrect estimation of the pressure dependence of the reaction rates, which may be particularly important for the isomerization reactions prevalent in low-temperature chemistry.

The third source of error may lie in the estimation of the thermodynamic properties of the species, particularly the fuel radicals. In the work of Diévar et al. [15], the program THERM [40] is used to estimate thermodynamic values using the group additivity method. In the RMG model constructed in this work, RMG itself estimates the thermodynamic properties of the molecules also using the group additivity method. Nonetheless, the two models have differing

331 predictions of the thermodynamic properties of the species in the model, par-  
 332 ticularly the fuel and its radicals. The values of the heats of formation of the  
 333 fuel and its H-atom abstraction radicals are shown in Table 3; the radicals are  
 334 labeled according to the convention shown in Fig. 6.



335

Figure 6: Structure of MV with carbon atoms labeled according to the convention used in  
 336 Table 3 and Table 4

Table 3: Heats of formation of MV and its radicals, labeled according to the convention used  
 337 in Fig. 6

| Radical Site | Diévert et al. [15] |            | RMG Model (this work) |            |
|--------------|---------------------|------------|-----------------------|------------|
|              | [kJ/mol]            | [kcal/mol] | [kJ/mol]              | [kcal/mol] |
| MV           | -470.98             | -112.57    | -472.53               | -112.94    |
| 2            | -297.16             | -71.02     | -273.63               | -65.40     |
| 3            | -277.03             | -66.21     | -273.63               | -65.40     |
| 4            | -277.03             | -66.21     | -278.61               | -66.59     |
| 5            | -265.94             | -63.56     | -267.53               | -63.94     |
| M            | -270.51             | -64.65     | -270.12               | -64.56     |

338

339 Table 3 shows that the heats of formation of the fuel and radicals 3, 4,  
 340 5, and M are quite similar between the two mechanisms. However, the heat  
 341 of formation of the second radical, the one closest to the methyl ester group,  
 342 has a significantly lower heat of formation in the model by Diévert et al. [15]  
 343 than in the RMG model. Note that it is expected that the second radical will  
 344 be somewhat more stable than the other radicals, due to the influence of the  
 345 methyl ester group on the adjacent carbon atom.

346 This difference in heats of formation affects the pathways that consume the  
 347 fuel. By conducting a reaction pathway analysis to determine which radicals



are formed from the breakdown of the fuel, we can analyze the proportion of each radical formed as the fuel breaks down during the autoignition process. The following analysis is conducted for a constant volume, adiabatic simulation with initial temperature and pressure of 700 K, 30 bar, and for the stoichiometric equivalence ratio. The rates of production of the species have been integrated until the time of 20 % fuel consumption. The results of this analysis are shown in Table 4 for the two models. The percentages shown in the Table 4 are the percent of the fuel consumed to form a particular fuel radical by all the reactions that can form that radical, and the radicals are labeled according to the convention in Fig. 6.

Table 4: Percent of MV consumed to form fuel radical species with a hydrogen atom missing at the location indicated in the first column and Fig. 6

| Radical Site | Diévert et al. [15] [%] | RMG Model [%] | RMG switched [%] |
|--------------|-------------------------|---------------|------------------|
| 2            | 29.2                    | 12.5          | 11.0             |
| 3            | 17.5                    | 12.2          | 11.1             |
| 4            | 17.5                    | 50.6          | 56.6             |
| 5            | 9.5                     | 3.9           | 4.3              |
| M            | 26.3                    | 20.8          | 16.9             |

At the relatively low temperature and high pressure condition of this analysis, all of the fuel is consumed by H-atom abstractions to form the fuel radicals shown. It can be seen that the two models have quite different distributions of products from the first H-abstraction reactions. The model of [15] predicts that H-abstraction from the second carbon is the most prevalent, while the RMG model predicts that the radical on the fourth carbon in the chain will be primarily formed. This is in line with the heats of formation in Table 3, where the most stable radical (i.e., the radical with the smallest heat of formation) is most likely to be formed in each model.

To further compare the models with each other, the NASA polynomials representing the thermodynamic properties of MV and the 5 fuel radicals from

the model of Diévar et al. [15] and are used to replace the equivalent molecules in the RMG model. The results of a path analysis at the same condition as the other analysis is shown in Table 4 in the “RMG switched” column. This analysis shows that the radical on the fourth carbon atom is still the most prevalent, despite changing the heats of formation of the fuel and its radicals.

Taken together, these results show that the poor performance in a given model cannot be attributed to a single source. There is a strong interaction between the thermodynamics of the species and the kinetics of the reactions, requiring further detailed study of the methyl ester system to accurately predict the low temperature ignition delays of methyl valerate.

## 6. Conclusions

In this study, we have measured ignition delays for methyl valerate over a wide range of engine-relevant pressures, temperatures, and equivalence ratios. An NTC region of the ignition delay and two-stage ignition are recorded for pressures of 15 bar at  $\phi = 2.0$  and 30 bar at  $\phi = 1.0$ . A detailed chemical kinetic model available in the literature is unable to reproduce the experimental results, so a new model is constructed using the Reaction Mechanism Generator software. Although the new model contains many more reactions than the literature model, it is still unable to predict the experimental ignition delays satisfactorily. Both models predict an NTC region of the ignition delay under conditions where none is found in the experiments, and fail to predict the NTC region of ignition delay that is present in the experiments. Possible reasons for the discrepancy include missing reaction pathways, incorrect rate estimates, and incorrect thermodynamic property estimates. Comparative analysis of the two models failed to identify a single source of the error, and further detailed studies are required to improve predictions of the ignition delay at these engine-relevant conditions.

## 399 References

- 400 [1] S. K. Hoekman, C. Robbins. Review of the effects of biodiesel  
 401 on NOx emissions. Fuel Processing Technology 96 (2012) 237–249.  
 402 doi:10.1016/j.fuproc.2011.12.036.
- 403 [2] J. Y. Lai, K. C. Lin, A. Violi. Biodiesel combustion: Advances in chemical  
 404 kinetic modeling. Progress in Energy and Combustion Science 37 (2011)  
 405 1–14. doi:10.1016/j.pecs.2010.03.001.
- 406 [3] L. Coniglio, H. Bennadji, P. Glaude, O. Herbinet, F. Billaud. Combustion  
 407 chemical kinetics of biodiesel and related compounds (methyl and  
 408 ethyl esters): Experiments and modeling – Advances and future refine-  
 409 ments. Progress in Energy and Combustion Science 39 (2013) 340–382.  
 410 doi:10.1016/j.pecs.2013.03.002.
- 411 [4] W. K. Metcalfe, S. Dooley, H. J. Curran, J. M. Simmie, A. M. El-Nahas,  
 412 M. V. Navarro. Experimental and modeling study of C<sub>5</sub>H<sub>10</sub>O<sub>2</sub> ethyl and  
 413 methyl esters. The Journal of Physical Chemistry A 111 (2007) 4001–4014.  
 414 doi:10.1021/jp067582c.
- 415 [5] S. M. Walton, M. S. Wooldridge, C. K. Westbrook. An experimental  
 416 investigation of structural effects on the auto-ignition properties of two  
 417 C<sub>5</sub> esters. Proceedings of the Combustion Institute 32 (2009) 255–262.  
 418 doi:10.1016/j.proci.2008.06.208.
- 419 [6] S. Dooley, H. J. Curran, J. M. Simmie. Autoignition mea-  
 420 surements and a validated kinetic model for the biodiesel surro-  
 421 gate, methyl butanoate. Combustion and Flame 153 (2008) 2–32.  
 422 doi:10.1016/j.combustflame.2008.01.005.
- 423 [7] B. Akih-Kumgeh, J. M. Bergthorson. Comparative Study of Methyl Bu-  
 424 tanoate and n -Heptane High Temperature Autoignition. Energy & Fuels  
 425 24 (2010) 2439–2448. doi:10.1021/ef901489k.

- 426 [8] B. Akih-Kumgeh, J. M. Bergthorson. Structure-reactivity trends of C1–C4  
427 alkanoic acid methyl esters. *Combustion and Flame* 158 (2011) 1037–1048.  
428 doi:10.1016/j.combustflame.2010.10.021.
- 429 [9] K. Hadj-Ali, M. Crochet, G. Vanhove, M. Ribaucour, R. Minetti. A study  
430 of the low temperature autoignition of methyl esters. *Proceedings of the*  
431 *Combustion Institute* 32 (2009) 239–246. doi:10.1016/j.proci.2008.09.002.
- 432 [10] K. Kumar, C.-J. Sung. Autoignition of methyl butanoate under en-  
433 gine relevant conditions. *Combustion and Flame* 171 (2016) 1–14.  
434 doi:10.1016/j.combustflame.2016.04.011.
- 435 [11] E. Fisher, W. J. Pitz, H. J. Curran, C. K. Westbrook. Detailed chem-  
436 ical kinetic mechanisms for combustion of oxygenated fuels. *Proceed-*  
437 *ings of the Combustion Institute* 28 (2000) 1579–1586. doi:10.1016/S0082-  
438 0784(00)80555-X.
- 439 [12] O. Korobeinichev, I. Gerasimov, D. Knyazkov, A. Shmakov, T. Bolshova,  
440 N. Hansen, C. K. Westbrook, G. Dayma, B. Yang. An Experimental and  
441 Kinetic Modeling Study of Premixed Laminar Flames of Methyl Pentanoate  
442 and Methyl Hexanoate. *Zeitschrift für Physikalische Chemie* 229 (2015).  
443 doi:10.1515/zpch-2014-0596.
- 444 [13] A. M. Dmitriev, D. A. Knyazkov, T. A. Bolshova, A. G. Shmakov,  
445 O. P. Korobeinichev. The effect of methyl pentanoate addition on  
446 the structure of premixed fuel-rich n-heptane/toluene flame at at-  
447 mospheric pressure. *Combustion and Flame* 162 (2015) 1964–1975.  
448 doi:10.1016/j.combustflame.2014.12.015.
- 449 [14] C. Hayes, D. R. Burgess. Exploring the oxidative decompositions of methyl  
450 esters: Methyl butanoate and methyl pentanoate as model compounds for  
451 biodiesel. *Proceedings of the Combustion Institute* 32 (2009) 263–270.  
452 doi:10.1016/j.proci.2008.05.075.

- [15] P. Diévar, S. H. Won, J. Gong, S. Dooley, Y. Ju. A comparative study of the chemical kinetic characteristics of small methyl esters in diffusion flame extinction. *Proceedings of the Combustion Institute* 34 (2013) 821–829. doi:10.1016/j.proci.2012.06.180.
- [16] G. Mittal, C.-J. Sung. A Rapid Compression Machine for Chemical Kinetics Studies at Elevated Pressures and Temperatures. *Combustion Science and Technology* 179 (2007) 497–530. doi:10.1080/00102200600671898.
- [17] G. Mittal, C.-J. Sung. Aerodynamics inside a rapid compression machine. *Combustion and Flame* 145 (2006) 160–180. doi:10.1016/j.combustflame.2005.10.019.
- [18] B. W. Weber, C.-J. Sung, in: S. Benthall, S. Rostrup (Eds.), *Proceedings of the 15th Python in Science Conference*, pp. 36–44. [http://conference.scipy.org/proceedings/scipy2016/bryan\\_weber.html](http://conference.scipy.org/proceedings/scipy2016/bryan_weber.html).
- [19] B. W. Weber, R. Fang, C.-J. Sung, UConnRCMPy, 2017. doi:10.5281/zenodo.269678.
- [20] D. G. Goodwin, H. K. Moffat, R. L. Speth, Cantera: An Object-oriented Software Toolkit for Chemical Kinetics, Thermodynamics, and Transport Processes, 2017. doi:10.5281/zenodo.170284.
- [21] S. van der Walt, S. C. Colbert, G. Varoquaux. The NumPy Array: A Structure for Efficient Numerical Computation. *Computing in Science & Engineering* 13 (2011) 22–30. doi:10.1109/MCSE.2011.37.
- [22] E. Jones, T. Oliphant, P. Peterson, et al., SciPy: Open source scientific tools for Python, 2001–. <https://scipy.org>.
- [23] J. D. Hunter. Matplotlib: A 2D Graphics Environment. *Computing in Science & Engineering* 9 (2007) 90–95. doi:10.1109/MCSE.2007.55.
- [24] D. Lee, S. Hochgreb. Rapid Compression Machines: Heat Transfer and Suppression of Corner Vortex. *Combustion and Flame* 114 (1998) 531–545. doi:10.1016/S0010-2180(97)00327-1.

- [25] J. Ortega, F. Espiau, J. Tojo, J. Canosa, A. Rodríguez. Isobaric Vapor-Liquid Equilibria and Excess Properties for the Binary Systems of Methyl Esters + Heptane. *Journal of Chemical & Engineering Data* 48 (2003) 1183–1190. doi:10.1021/jc030117d.
- [26] A. C. van Genderen, J. van Miltenburg, J. G. Blok, M. J. van Bommel, P. J. van Ekeren, G. J. van den Berg, H. A. Oonk. Liquid–vapour equilibria of the methyl esters of alkanolic acids: Vapour pressures as a function of temperature and standard thermodynamic function changes. *Fluid Phase Equilibria* 202 (2002) 109–120. doi:10.1016/S0378-3812(02)00097-3.
- [27] S. P. Verevkin, V. N. Emel’yanenko. Transpiration method: Vapor pressures and enthalpies of vaporization of some low-boiling esters. *Fluid Phase Equilibria* 266 (2008) 64–75. doi:10.1016/j.fluid.2008.02.001.
- [28] A. G. Camacho, J. M. Moll, S. Canzonieri, M. A. Postigo. Vapor-Liquid Equilibrium Data for the Binary Methyl Esters (Butyrate, Pentanoate, and Hexanoate) (1) + Propanenitrile (2) Systems at 93.32 kPa. *Journal of Chemical & Engineering Data* 52 (2007) 871–875. doi:10.1021/jc060469v.
- [29] R. M. Stephenson, S. Malanowski, D. Ambrose, *Handbook of the Thermodynamics of Organic Compounds*, Elsevier, New York, 1987.
- [30] E. E. Dames, A. S. Rosen, B. W. Weber, C. W. Gao, C.-J. Sung, W. H. Green. A detailed combined experimental and theoretical study on dimethyl ether/propane blended oxidation. *Combustion and Flame* 168 (2016) 310–330. doi:10.1016/j.combustflame.2016.02.021.
- [31] A. C. Hindmarsh, P. N. Brown, K. E. Grant, S. L. Lee, R. Serban, D. E. Shumaker, C. S. Woodward. SUNDIALS: Suite of nonlinear and differential/algebraic equation solvers. *ACM Transactions on Mathematical Software* 31 (2005) 363–396. doi:10.1145/1089014.1089020.
- [32] S. C. Chapra, R. P. Canale, *Numerical Methods for Engineers*, McGraw-Hill Higher Education, Boston, 6th ed edition, 2010.

- [33] J. W. Allen, C. F. Goldsmith, W. H. Green. Automatic estimation of pressure-dependent rate coefficients. *Physical Chemistry Chemical Physics* 14 (2012) 1131–1155. doi:10.1039/c1cp22765c.
- [34] B. W. Weber, C.-J. Sung, M. W. Renfro. On the uncertainty of temperature estimation in a rapid compression machine. *Combustion and Flame* 162 (2015) 2518–2528. doi:10.1016/j.combustflame.2015.03.001.
- [35] B. W. Weber, K. E. Niemeyer. ChemKED: A human- and machine-readable data standard for chemical kinetics experiments. Submitted to: *International Journal of Chemical Kinetics* (2017). [arXiv:1706.01987](https://arxiv.org/abs/1706.01987).
- [36] G. Kukkadapu, K. Kumar, C.-J. Sung, M. Mehl, W. J. Pitz. Experimental and surrogate modeling study of gasoline ignition in a rapid compression machine. *Combustion and Flame* 159 (2012) 3066–3078. doi:10.1016/j.combustflame.2012.05.008.
- [37] M. Ribaucour, R. Minetti, L. R. Sochet. Autoignition of n-pentane and 1-pentene: Experimental data and kinetic modeling. *Symposium (International) on Combustion* 27 (1998) 345–351. doi:10.1016/S0082-0784(98)80422-0.
- [38] J. Bugler, K. P. Somers, E. J. Silke, H. J. Curran. Revisiting the Kinetics and Thermodynamics of the Low-Temperature Oxidation Pathways of Alkanes: A Case Study of the Three Pentane Isomers. *The Journal of Physical Chemistry A* 119 (2015) 7510–7527. doi:10.1021/acs.jpca.5b00837.
- [39] K. A. Heufer, J. Bugler, H. J. Curran. A comparison of longer alkane and alcohol ignition including new experimental results for n-pentanol and n-hexanol. *Proceedings of the Combustion Institute* 34 (2013) 511–518. doi:10.1016/j.proci.2012.05.103.
- [40] E. R. Ritter, J. W. Bozzelli. THERM: Thermodynamic property estimation for gas phase radicals and molecules. *International Journal of Chemical Kinetics* 23 (1991) 767–778. doi:10.1002/kin.550230903.